Sonodynamic Therapy Complements PD-L1 Immune Checkpoint Inhibition in a Murine Model of Pancreatic Cancer.

Heather Nesbitt[1], Keiran Logan[1], Keith Thomas[1], Bridgeen Callan[1], Jinhui Gao[1], Thomas McKaig[1], Mark Taylor[2], Mark Love[3], Eleanor Stride,[4] Anthony P. McHale[1], John F. Callan[1*]

1. Biomedical Sciences Research Institute, University of Ulster, Coleraine, Northern Ireland, UK; 2. Department of HPB Surgery, Mater Hospital, Belfast, Northern Ireland, U.K. BT14 6AB. 3. Imaging Centre, The Royal Victoria Hospital, Grosvenor Road, Belfast, Northern Ireland, U.K. BT12 6BA; 4. Institute of Biomedical Engineering, University of Oxford, Oxford, U.K. OX3 7DQ.

* Corresponding author. Biomedical Sciences Research Institute, University of Ulster, Coleraine, Northern Ireland, UK. Email address: j.callan@ulster.ac.uk.

Abstract: The emergence of immune checkpoint inhibitors (ICI's) in the past decade has proven transformative in the area of immuno-oncology. The PD-1 / PD-L1 axis has been particularly well studied and monoclonal antibodies developed to block either the receptor (anti PD-1) or its associated ligand (anti PD-L1) can generate potent anti-tumour immunity in certain tumour models. However, many "immune cold" tumours remain unresponsive to ICI's and strategies to stimulate the adaptive immune system and make these tumours more susceptible to ICI treatment are currently under investigation. Sonodynamic therapy (SDT) is a targeted anti-cancer treatment that uses ultrasound to activate a sensitiser with the resulting generation of reactive oxygen species (ROS) causing direct cell death by apoptosis and necrosis. SDT has also been shown to stimulate the adaptive immune system in a pre-clinical model of colorectal cancer. In this manuscript, we investigate the ability of microbubble mediated SDT to control tumour growth in a bilateral tumour mouse model of pancreatic cancer by treating the target tumour with SDT and observing the effects at the off-target untreated tumour. The results demonstrated a significant 287% decrease in tumour volume when compared to

untreated animals 11 days following the initial treatment with SDT, which reduced further to 369% when SDT was combined with anti-PD-L1 ICI treatment. Analysis of residual tumour tissues remaining after treatment revealed increased levels of infiltrating $CD4^+$ and $CD8^+$ T-lymphocytes (respectively 4.65 and 3.16-fold more) in the off-target tumours of animals where the target tumour was treated with SDT and anti-PD-L1, when compared to untreated tumours. These results suggest that SDT treatment elicits an adaptive immune response that is potentiated by the anti-PD-L1 ICI in this particular model of pancreatic cancer.

Keywords: Sonodynamic therapy, immune checkpoint inhibitor, PD-L1, pancreatic cancer.

1. Introduction: Significant progress has been made in the area of immuno-oncology over the past decade with several immune checkpoint inhibitors (ICI) now approved for clinical use [1,2]. Immune checkpoints help regulate T-cell function and protect the host against autoimmunity [3]. Unfortunately, cancer cells often exploit these checkpoints to suppress effector T-cell function resulting in evasion of immune surveillance [4,5]. Essentially ICI's function by blocking this signalling interaction between T-cells and tumour cells enabling the T-cells to exert their cytotoxic effect against the tumour cells [6]. The programmable death protein (PD-1) and its associated ligand PD-L1, is a well-studied immune checkpoint and monoclonal antibodies have been developed to recognise and bind to either PD-1 (nivolumab, pembrolizumab and cemiplimab) or PD-L1 (atezolizumab, avelumab and durvalumab) [7-10]. While impressive outcomes have been achieved in certain groups of patients treated with ICI's, the response rate remains variable [11]. Combining ICI's with other treatment modalities has also been explored, particularly those that complement the ICI's mechanism of action. For example, treatment of a primary lesion with ionizing radiation has resulted in tumour control at a distant untreated metastatic site, an effect attributed to activation of the adaptive immune system and referred to as an "abscopal effect" [12, 13]. Several pre-clinical studies have demonstrated the benefit of combining ICIs with radiotherapy and clinical trials exploring this

combination are currently in progress [14]. Similarly, photodynamic therapy (PDT) has been shown to stimulate an adaptive immune response and several pre-clinical studies have demonstrated therapeutic benefit when combined with ICI's [15, 16, 17]. Unfortunately, the utility of PDT as a clinical treatment has been limited to superficial lesions due to the inability of visible light to penetrate deeply into human tissue [18,19,20]. While near infrared (NIR) absorbing photosensitisers [21, 22] and multi-photon excitation strategies [23, 24] have offered some improvement in this area, achieving sensitiser activation at depths in excess of 1 cm in human tissue remains a challenge.

Sonodynamic therapy (SDT) is similar to PDT with the exception that it uses low-intensity ultrasound instead of light to activate the sensitiser [25]. In both PDT and SDT, the activated sensitiser interacts with molecular oxygen and / or biological substrates to generate reactive oxygen species (ROS) that induce cell death by apoptosis and necrosis [26]. Low intensity ultrasound is widely used in medicine and can penetrate tens of centimetres through soft tissue, enabling the activation of sensitisers at a much greater depth than can be achieved using light [27]. As the sensitiser and ultrasound stimulus are harmless on their own, SDT is a targeted therapy with limited systemic side effects making it better tolerated than other cancer treatments such as chemotherapy and radiotherapy. The efficacy of SDT has been demonstrated in a range of different cancer types and a recent study has also shown the ability of this treatment to elicit an abscopal effect in a murine model of liver cancer [28]. We have previously demonstrated the potential of SDT in a range of pre-clinical pancreatic cancer models and hypothesise that ICI's may complement SDT in the treatment of pancreatic cancer [29-31].

Survival rates for pancreatic cancer have barely changed in over 40 years and new approaches to the treatment of this disease are highly sought after. While clinical studies investigating the potential of anti-PD-L1 in pancreatic cancer have been few and generally inconclusive, pre-clinical studies have yielded more encouraging results [32,33]. A significant challenge in the treatment of pancreatic cancer is the dense protective tumour stroma that can

act as a barrier for the access of drugs and infiltrating T-cells [34-36]. To enhance the effectiveness of SDT treatment, we routinely attach the sensitiser to the surface of lipid stabilised microbubbles [31,37]. Irradiation of tumours with low-intensity ultrasound during systemic administration of the sensitiser-microbubble conjugate, causes inertial cavitation and enhanced activation of the sensitiser, an approach referred to as ultrasound targeted microbubble destruction (UTMD) [31,37]. An additional benefit of this approach is that cavitation is known to promote microscale mass transport though impermeable tissue, and this may also improve sensitiser delivery across the tumour stroma [38,39].

In this manuscript, we investigate the ability of SDT to generate an abscopal response in a T110299 mouse model of pancreatic cancer. Bilateral T110299 tumours were established in immunocompetent mice and one tumour treated with ultrasound during systemic administration of a microbubble-Rose Bengal conjugate (MB-RB). The response of both the SDT treated and untreated tumours was evaluated in the presence and absence of an anti-PD-L1 antibody. The infiltration of CD4+ and CD8+ T cells into residual tumour tissues at the end of the experiment was also determined to identify a potential correlation between T-lymphocyte tumour infiltration and treatment outcome.

2. Materials and Methods

2.1 *Materials and Reagents*: 1,2-dibehenoyl-sn-glycero-3-phosphocholine (DBPC), 1,2-distearoyl-sn-glycero-3-phosphoethanolamine-N-[methOxy(polyethylene glycol) -2000] (DSPE-PEG (2000)), and DSPE-PEG (2000)-biotin were purchased from Avanti Polar Lipids (Alabaster, AL, USA). Perfluorobutane (PFB) was purchased from Apollo Scientific Ltd (Cheshire, UK). Glycerol, propylene glycol, 3-(4,5-dimethylthiazol-2-yl)-2,5-diphenyltetrazolium bromide (MTT), avidin (egg white), Tween 20, Paraformaldehyde (PFA), tri-sodium citrate and ethanol were purchased from Sigma Aldrich (St. Louis, MO, USA) at the highest grade possible. Biotin functionalised Rose Bengal (Biotin-RB) was prepared according

to ref 37. Microbubbles were formed using a Microson ultrasonic cell disruptor, 100 W, 22.5 kHz, from Misonix Inc. (NY, USA). The T110299 cell line, a gift from Prof. Jens Siveke, (Klinikum rechts der Isar, Technical University Munich, Munich, Germany), was isolated from primary pancreatic tumours in KPC mice (Ptfla-Cre; LSL-KrasG12D; LSL-Trp53fl/R172H) [41]. Propidium iodide (0.05 µg/test, Molecular Probes), 4′,6-diamidino-2-phenylindole (DAPI), Bovine Serum Albumin (BSA), Matrigel® (Corning), Phosphate buffered saline (PBS) (Gibco), RPMI (Gibco), Fetal Bovine Serum (FBS) (Gibco), collagenase type II (Gibco), DNAse (Gibco), fluorochrome conjugated antibodies specific for CD45 (PE-Cy7/0.125µg/test, eBioscience), CD3 (APC-eFluro 780/0.5 µg/test, eBioscience), CD4 (Alexa Fluor 700/0.125 µg/test, eBioscience) and CD8a (PE/0.25 µg/test, eBioscience) and multi-species RBC lysis buffer (eBioscience) were purchased from Thermo Fisher Scientific (Abingdon, UK). Anti-Calreticulin (ab196159) conjugated antibody was purchased from Abcam (Cambridge, UK). Optical microscope images were obtained using a Leica DM500 optical microscope. Fluorescence images of microbubbles were taken using a Nikon Eclipse E400 epi-fluorescence microscope (Minato City, Tokyo, Japan) equipped and the G-2A longpass emission filter set (λ_{EX} 510–560, 80% transmission with a 590 nm cut-off wavelength of the longpass emission). Fluorescence microscope images of cells were taken using an Olympus System BX51 Microscope (Shinjuku City, Tokyo, Japan). C57BL/6JOlaHsd mice were purchased from Envigo (Blackthorn, England). Ultrasound treatments were delivered using a Sonidel SP100 sonoporator (Sonidel Limited, Dublin Ireland). Flow cytometry analysis of cell suspensions was performed using a Gallios flow cytometer (Beckman Coulter, Brea, CA, USA) and analysed using FlowJo software with gating established on unstained controls or Igκ single stained compensation controls, as appropriate.

2.2 Preparation of O_2 MB-RB: Preparation of MB-RB followed the protocol described in ref 34 with the exception that DBPC was used in place of DSPC. Briefly, avidin-functionalised MB were prepared by first dissolving DBPC (4.0 mg, 4.44 µmol), DSPE-PEG(2000) (1.35 mg, 0.481 µmol) and DSPE-PEG(2000)-biotin (1.45 mg, 0.481 µmol) in chloroform to achieve a

molar ratio of 82:9:9. (Scheme 1) The solvent was evaporated and the lipid film was then reconstituted in 2 mL of a solution containing PBS, glycerol and propylene glycol (8:1:1 vol ratio) (PPG) and heated in a water bath at 80 °C for 30 min. The suspension was sonicated using in a perfluorobutane (PFB) atmosphere for 30 sec to afford a milky white suspension of MBs. The MBs were then washed by centrifugation (100 RCF) and the infranatant replaced with PPG (2 mL). The MB cake was then mixed for 5 min on ice with an aqueous solution of avidin (10 mg/mL). The resulting avidin-MBs were washed as described previously and the MBs mixed for 5 min with an aqueous solution containing biotin-RB (5 mg/mL, 1 mL) before further washing of the MBs. The final MB number was determined on a haemocytometer using an optical microscope. Size distribution analysis was carried out using a customised MATLAB algorithm [40]. O_2MB-RB were prepared by oxygenating immediately prior to use by sparging with O_2 gas for 2 min. The drug loading of O_2MB-RB was determined using UV–Vis spectroscopy following destruction of a sample of MBs using ultrasound and then measuring the RB absorbance at 560 nm. The drug loading was determined as 33.5 ± 4.3 μg per 10^8 MBs.

2.3 CRT expression in T110299 cells treated with sonodynamic therapy: T110299 cells ($1X10^4$) were seeded in a 4 well Lab-Tek II chamber and incubated overnight. Cells were treated with ultrasound alone and O_2MB-RB (10 μM RB, $3.70x10^7$ MB/mL) in the presence or absence of ultrasound (3.0 Wcm^{-2}, 1 MHz, 50% duty cycle, 20 seconds). After 3 hours, cells were washed twice with PBS and the media replaced. 24 hours later cells were fixed in 4% PFA and antigen retrieved with citrate buffer for 15 min at 95^{o}C. Citrate buffer consisted of 2.94 g of tri-sodium citrate in 1 L of distilled water supplemented with 0.5 mL Tween20. Cells were blocked in 5% BSA for 3 hours. Anti-Calreticulin (ab196159) conjugated antibody was diluted in 5% BSA (1:500). Cells were incubated in antibody at 4^{o}C overnight. Cells were washed twice with PBS and stained with DAPI for 1 min. Cells were washed, cover slipped and viewed under tetramethylrhodamine isothiocyanate filter (594 nm) using a fluorescent

microscope and photographed using the DP70 camera adapter system. Image J software was used to quantify fluorescence intensity per cell for all treatment groups.

2.4 Cytotoxicity of sonodynamic therapy and immunotherapy in-vivo: All animals employed in this study were treated in accordance with the licensed procedures under the UK Animals (Scientific Procedures) Act 1986. T110299 cells in were subcutaneously implanted in the right and left rear dorsum of C57BL/6JOlaHsd mice. Each implant contained $5x10^5$ cells in 100 µl Matrigel® High Concentration. Tumours were apparent approximately 1 week after implantation. Tumour volume was measured using Vernier callipers using the equation tumour (width x length x height)/2. When tumours reached an average volume of 150 mm^3, the animals were distributed into four groups (n=5). (Figure 1) Group 1 (SDT + PDL-1) received an intraperitoneal injection (IP; 10mg/kg) of *InVivo*MAb anti-mouse PD-L1 antibody (B7-H1, 2BScientific). After 2 hours, mice in this group also received an intravenous (IV) tail vein injection (100 µL) of O_2MB-RB suspension ($1.57 \times 10^9 \pm 1.19 \times 10^8$ MB/mL, [RB-biotin] = 2.63 ± 0.34 mg/kg) while simultaneously receiving ultrasound (3.5 Wcm^{-2}, 1 MHz, 30% duty cycle, and PRF = 100 Hz; PNP = 0.48 MPa; MI = 0.48) applied to the right-hand-side (target) tumour (Figure 1) during and after injection (for a total of 3.5 min), with a second 3.5 min ultrasound exposure 30 min following injection; Group 2 (SDT) received the same MB and ultrasound treatment as Group 1 but no anti PD-L1 antibody was administered to these animals; Group 3 (PDL-1) received anti-PD-L1 antibody alone and Group 4 (Untreated) remained untreated. The first ultrasound treatment was to cause MB inertial cavitation and the second, 30 minutes later was to activate the Rose Bengal SDT treatment. Tumour volume and mouse weight were measured daily following the initial treatment. Mice were treated on days 0, 4 and 7. For groups 1 and 2, the “target tumour” was the right-hand-side tumour that received ultrasound treatment (i.e. SDT) while the left-hand-side tumour was designated the off-target. However, for groups 3 and 4, no tumour received SDT treatment and therefore the designations of target and off-target were not appropriate.

2.5 Preparation of tumour samples for flow cytometry: On day 11 animals were sacrificed from the study described in Section 2.4, residual tumour tissues were excised and homogenised into single cell suspensions in RPMI supplemented with 4% FBS, 160 µL (30 mg/mL) collagenase type II, 50 µL (2 µg/mL) DNAse and incubated at room temperature in a high-speed shaker for 15 min. The mixture was filtered through a 100 µm filter, centrifuged at 17000 rpm for 5 mins and supernatant was decanted. Cells were washed twice in ice cold PBS. Subsequently cells were stained extracellularly with propidium iodide (0.05 µg/test) for viability determination and fluorochrome conjugated antibodies specific for CD45 (PE-Cy7/0.125µg/test), CD3 (APC-eFluro 780/0.5 µg/test), CD4 (Alexa Fluor 700/0.125 µg/test) and CD8a (PE/0.25 µg/test), in PBS containing 0.2% (w/v) bovine serum albumin for 30 minutes at RT. Red blood cells were removed using multi-species RBC lysis buffer as per manufacturer's instructions. Viable cells were determined as propidium iodide negative and single were identified by plotting FS-H versus FS-A. Cytotoxic T cells were identified as $CD45^{+}CD3^{+}CD8a^{+}$ cells. Helper T cells were identified as CD45+CD3+CD4+ cells. Data generated was analysed using FlowJo, with fold-change in treatment groups calculated in comparison to untreated. The gating strategy is summarised in the table below.

PBMCs	CD45	CD3	CD4	CD8a
T Helper	+	+	+	-
Cytotoxic	+	+	-	+

2.6 Statistics: Statistical analysis was carried out using GraphPad prism 5 for Windows. Data were analysed using a 2 tailed, unpaired t-test. * denotes $p<0.05$, ** denotes $p<0.01$, *** denotes $p<0.001$, ns denotes no significance.

3. Results and Discussion: Lipid stabilised MBs loaded with Rose Bengal (MB-RB) were prepared following the approach outlined in our previous work [37]. Briefly, this involved sonicating an aqueous dispersion of the phospholipids DBPC, DSPE-PEG(2000) and DSPE-PEG (2000)-biotin under a headspace of PFB gas to generate MBs with biotin units protruding from the MB shell. Avidin was then used to cross-link the biotin functionalised MBs to a previously prepared biotin-RB ligand generating the final MB-RB formulation. The MBs were characterised using optical and fluorescence microscopy and representative images are shown in Figure 2 (A and B). Spherical particles with a mean diameter of 2.06 ± 0.27 µm and a mean MB concentration of $1.57 \times 10^9 \pm 1.19 \times 10^8$ MB/mL were obtained that emitted red fluorescence from their shells when excited at 510-560 nm (λ_{EX} = 555 nm, λ_{EM} = 582 nm) confirming attachment of the weakly fluorescent RB (Figure 2B).

Calreticulin (CRT) is a protein which is found on the surface of cells and is commonly used as a marker for immunogenic cell death (ICD) [28]. To probe the effect of MB-RB mediated SDT treatment on the expression of CRT, a suspension of MB-RB was added to T110299 cells and then subjected to ultrasound treatment. Cells treated with MB-RB or ultrasound only were used for comparative purposes. CRT expression was quantified using an Alexa Fluor 647 labelled anti-CRT antibody added to the cells following treatment. Fluorescent microscope images of the treated cells (Figure 3a) showed intense red fluorescence associated with the membrane region of the cells (i.e. non-nucleus) exposed to SDT which was 3 times more intense than cells treated with MB-RB or ultrasound alone($p<0.001$). This increased fluorescence intensity can be attributed to enhanced CRT expression suggesting SDT treatment induces ICD in T110299 cells.

Tumours were established in the rear left and right-hand flanks of immunocompetent C57 mice using the T110299 cell line. Tumours generated from this cell line have similar histological characteristics as primary KPC murine tumours as they carry Kras and p53 mutations, have extensive stromal development, are poorly vascularised and display a highly immunosuppressive tumour microenvironment [41]. To investigate the effect of UTMD

mediated SDT treatment in this model of pancreatic cancer, a suspension of O_2MB-RB was administered intravenously, and ultrasound applied to the chosen target tumour but not to the off-target tumour (opposite flank) (Figure 1). Following UTMD mediated SDT treatment, the tumour volume at both the target and off-target tumours was measured daily and the results are shown in Figure 4. When compared with tumour volumes observed in untreated animals, a significant 348% reduction in tumour volume was observed for the primary tumour 11 days after the initial treatment indicating a strong SDT mediated anti-tumour effect ($p \leq 0.01$). Interestingly, a significant 287% decrease in tumour volume was also observed for the off-target tumour at the same timepoint ($p \leq 0.01$). Since singlet oxygen and ROS have short lifetimes and diffusion distances [42], the reduction in tumour volume observed at the distant tumour cannot be due to direct SDT mediated toxicity, but most likely results from an immune-mediated abscopal effect.

To investigate this interaction further and determine if anti-PD-L1 ICI could enhance the effect of UTMD SDT observed at the distant tumour, the previous experiment was repeated with animals exposed to anti-PD-L1 treatment 2 hours prior to UTMD SDT treatment. Treatment with anti-PD-L1 alone resulted in a 266% reduction in tumour volume (average values from both tumours on a single animal) when compared with tumour volumes on untreated animals, 11 days after the initial treatment ($p \leq 0.01$) (Figure 4B). When anti-PD-L1 treatment was combined with UTMD mediated SDT, the reduction observed at the target and off-target tumours were 352% and 369% respectively. When the effects of SDT, anti-PD-L1 and combined SDT / anti-PD-L1 treatment on the off-target tumour were considered separately (Figure 5A), a substantial improvement in tumour reduction was observed for the combination treatment when compared to SDT or anti-PD-L1 treatment alone. This was further supported by the observation that, at the end of the experiment, the tumour mass from animals treated with the combination was significantly lower ($p<0.05$) than that from animals receiving either treatment alone (Figure 5B).

The results described above suggest that SDT treatment of the target tumour induces an abscopal effect at the off-target tumour, which is enhanced or complemented by anti-PD-L1 ICI therapy. One possible explanation for this effect is that like PDT, SDT induced cell death stimulates an adaptive immune response mediated by release of cell death-associated molecular patterns (CDAMPs) or damage-associated molecular patterns (DAMPs), triggering the maturation of dendritic cells [43]. The mature dendritic cells then migrate to the lymph nodes where they present antigens to $CD4^+$ (T helper cells) or CD8 T^+ (cytotoxic T cells) cells. The activated T cells return to the circulation and infiltrate the tumour where they can influence immunogenic cell death [4]. Unfortunately, the PD-1 / PD-L1 checkpoint can inhibit T cell activation and instead cause apoptosis of cytotoxic T cells [45, 46]. By blocking this pathway using anti-PD-L1, more CD8 cells can become activated and infiltrate the tumour. Flow-cytometry analysis of residual tumour tissues excised at the end of the study support this hypothesis as a significant increase (1.80 fold, $p<0.05$) in $CD8^+$ cells was present in the off-target tumours of animals treated with SDT. (Figure 7) Indeed, when SDT was combined with anti-PD-L1 treatment, CD8+ cell infiltration increased further at the off-target tumour (3.16 fold, $p <0.001$), consistent with the improvement observed for this group in the tumour growth delay study. Increased tumour levels of $CD8^+$ and $CD4^+$ T cells have been identified as a positive prognostic indicator of survival in patients with borderline resectable pancreatic cancer following neoadjuvant chemoradiation treatment [47]. Encouragingly, $CD4^+$ and $CD8^+$ cells were found to be elevated in the off-target tumours of animals treated with combined SDT / anti-PD-L1 treatment, indicating a strong systemic immunogenic effect with the potential to control metastatic disease.

In conclusion, microbubble mediated SDT treatment of a target tumour in a bilateral tumour model of pancreatic cancer, enables growth control at both the target and off-target tumours which is further enhanced when combined with anti-PD-L1 ICI treatment. Increased levels of tumour infiltrating CD4+ and CD8+ cells were evident in off-target tumours treated with combined SDT / anti-PD-L1, suggesting that inhibition of tumour growth resulted from

activation of the adaptive immune system. Pancreatic cancer remains one of the most difficult cancers to treat and aggressive chemotherapy combinations such as gemcitabine / Abraxane or FOLFIRINOX produce only modest survival benefit and are associated with significant off-target side effects [48, 49]. In contrast, the ROS generation in SDT can be targeted by control of the ultrasound stimulus, implying that it would be generally well tolerated [30,50]. Therefore, combining SDT with anti-PD-L1 ICI treatment, which is also well tolerated [33], could provide an attractive treatment option for pancreatic cancer, particularly for patients with advanced disease who may not be physically capable of undertaking a toxic chemotherapy regimen.

Acknowledgements

JFC thanks Norbrook Laboratories Ltd for an endowed chair.

Authors Contribution

HN carried out the in-vivo and immuno-fluorescence study. KL, JG and TK assisted with microbubble preparation and animal treatments. KT ran flow cytometry and analysed data. All authors were involved in reviewing and editing the manuscript.

Figures & Diagrams

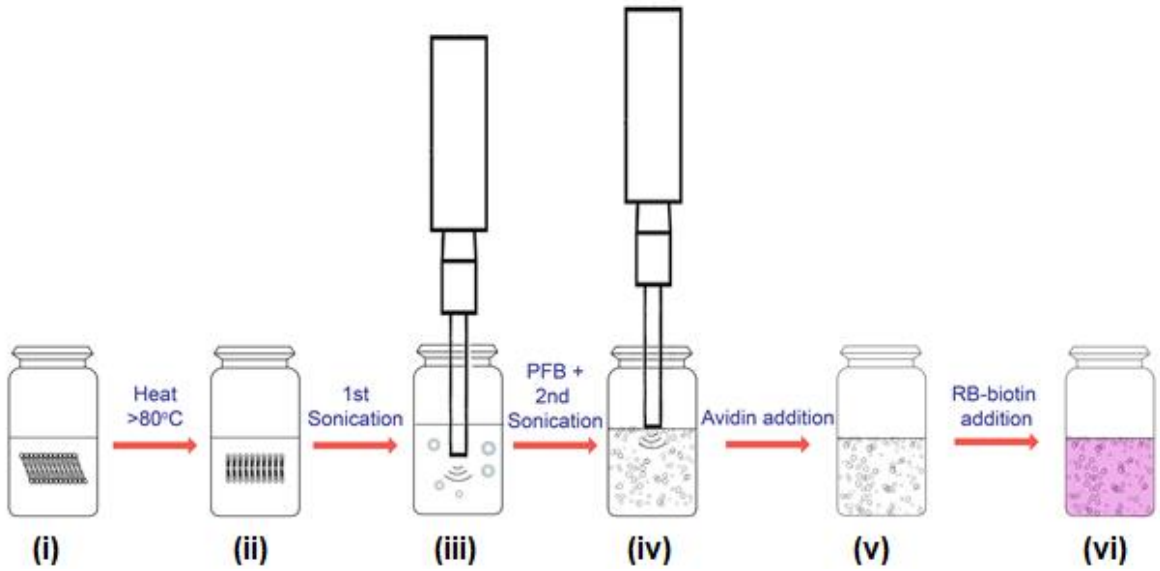

Scheme 1 Schematic illustration for the preparation of O_2MB-RB. A hydrated lipid film (i) was heated above its lipid phase temperature (ii) and then sonicated (iii). It was then cooled and sonicated under an atmosphere of PFB (iv) to form the MB. The MB were then mixed with avidin (v) and then RB-biotin (vi) which following sparging with O_2 gas produced the O_2MB-RB.

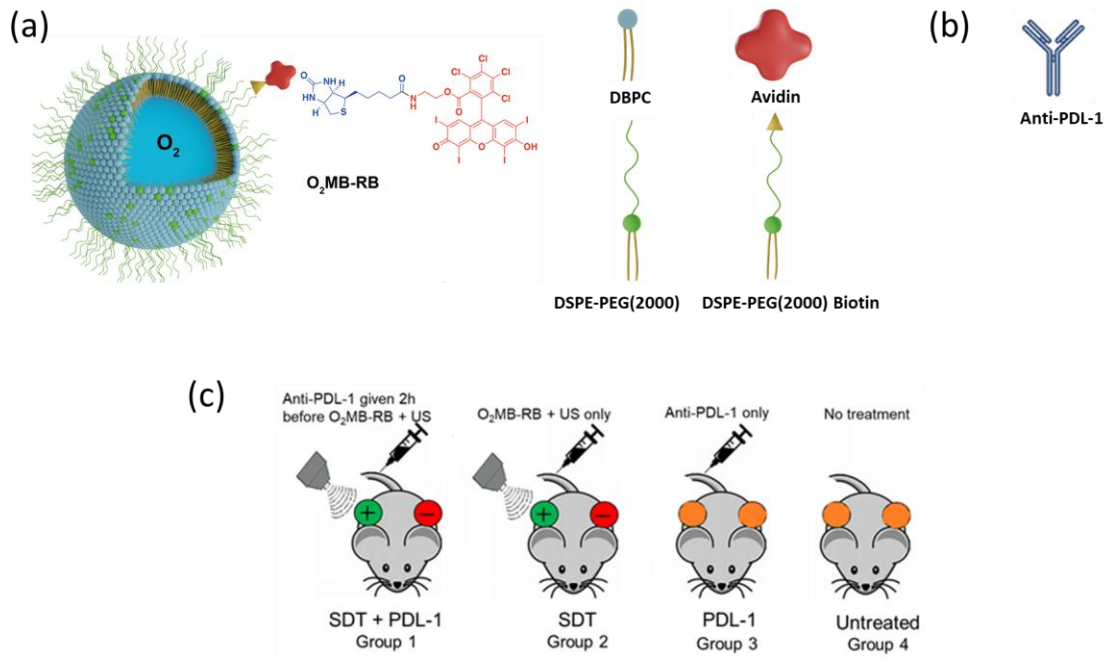

Figure 1 Schematic representation of (a) the MB-RB conjugate and (b) anti-PDl-1. (c) Schematic representation outlining the treatment groups used during the animal study. In groups 1 and 2, the right-hand-side tumour (green +) was designated the target tumour as this received SDT treatment and the left-hand-side tumour (red -) the off-target tumour. In groups 3 and 4, neither tumour was treated with SDT and therefore this designation was not used.

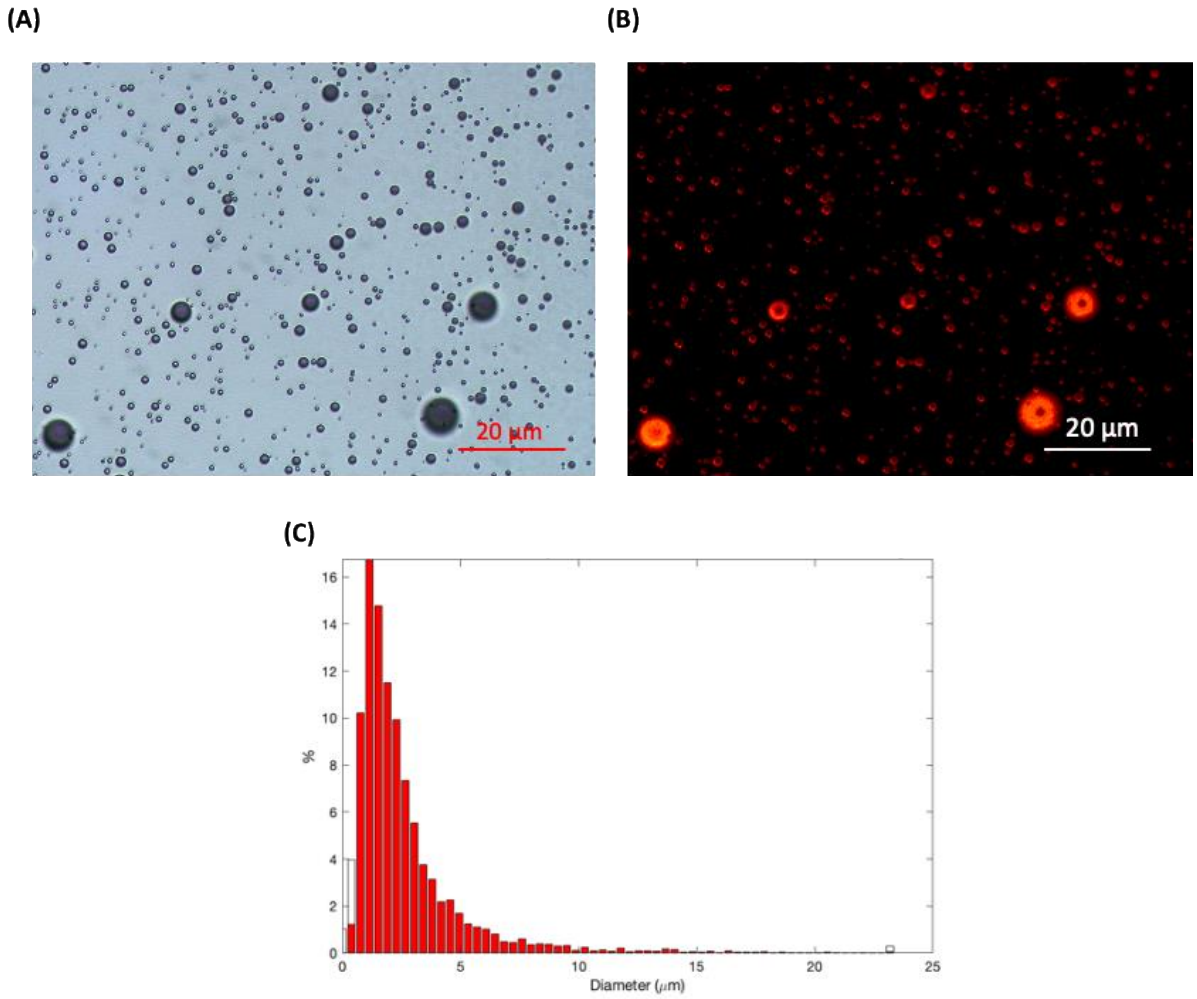

Figure 2 (A) Brightfield optical microscopy image of MB-RB (B) Fluorescence microscopy image of RB-MB (C) Size distribution plot for MB-RB (n = 20 images).

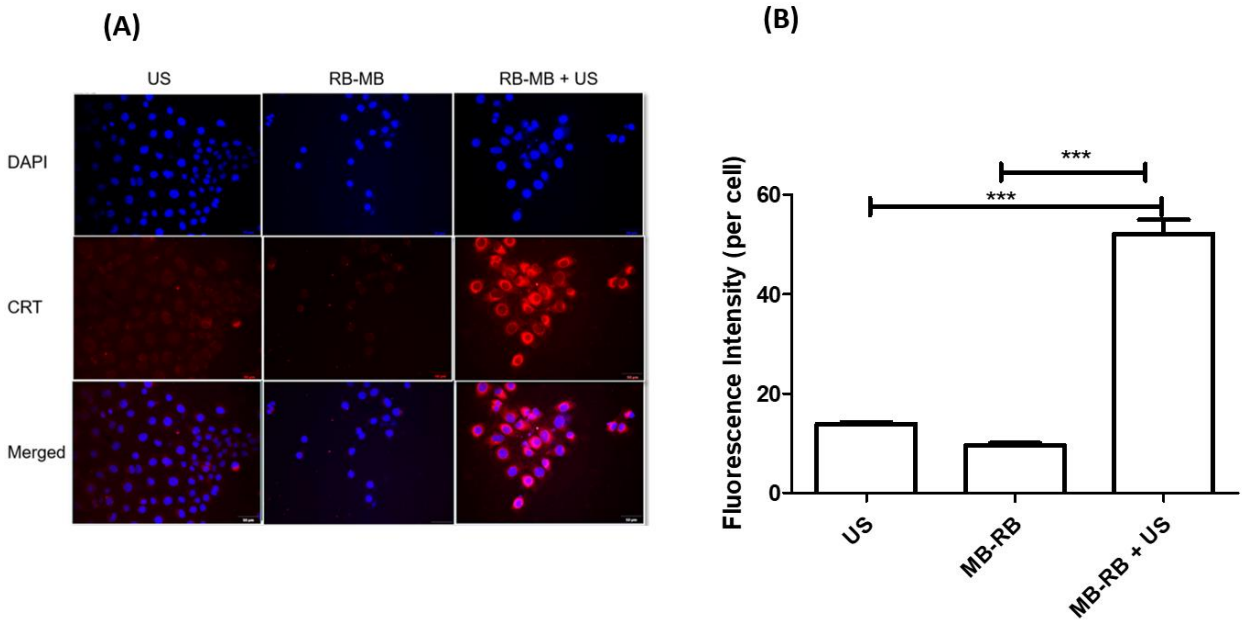

Figure 3 DAPI, CRT and merged images for KPC cells treated with MB-RB in the presence of ultrasound. Cells were stained with Alexa Fluor 647-CRT and DAPI and imaged under a fluorescent microscope (Olympus System Microscope, model BX51; Southend-on-Sea, UK).

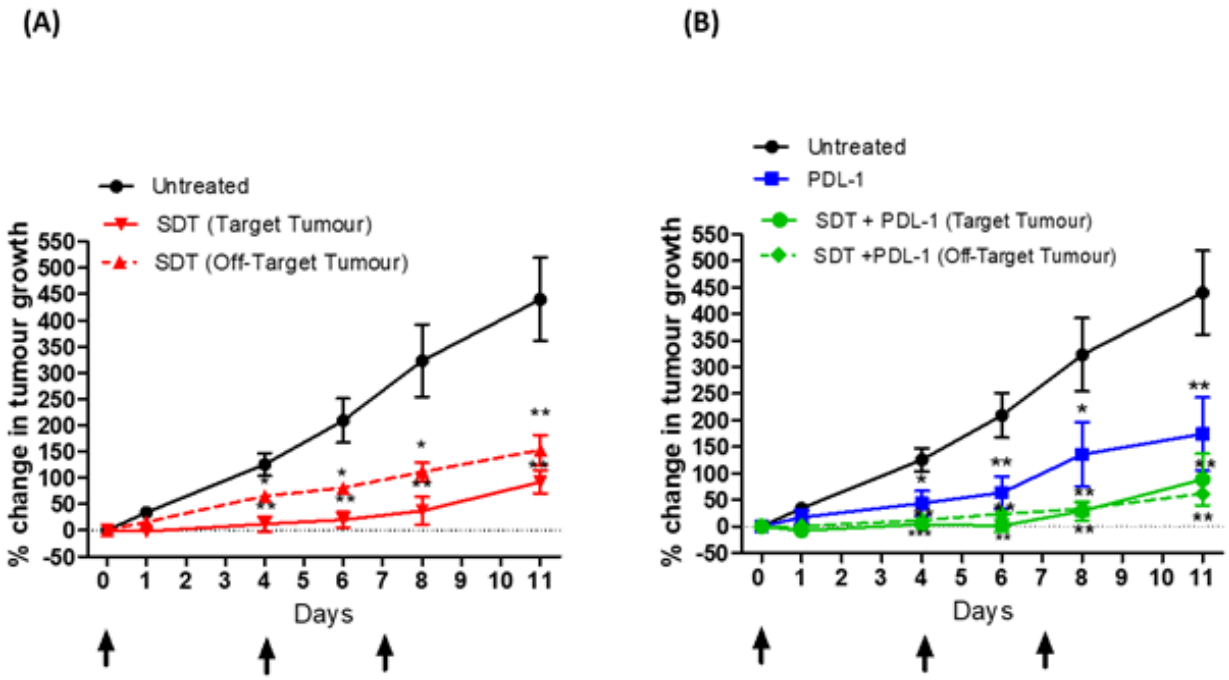

Figure 4 Plot of % tumour volume against time for mice bearing ectopic bilateral T110299 pancreatic tumours with (A) one tumour treated with the O_2MB-RB + US (Target Tumour) while the second tumour remained untreated (Off-target Tumour). (B) tumours received (i) no treatment (ii) an injection of anti-PD-L1 antibody (iii) an injection of anti-PD-L1 antibody 2h before treatment of the target tumour with the O_2MB-RB + US (anti-PD-L1 + SDT). Animals were treated on Days 0, 4 & 7. *$p \leq 0.05$, **$p \leq 0.01$ for comparison to untreated animals Error bars represent ± SEM where $n \geq 4$.

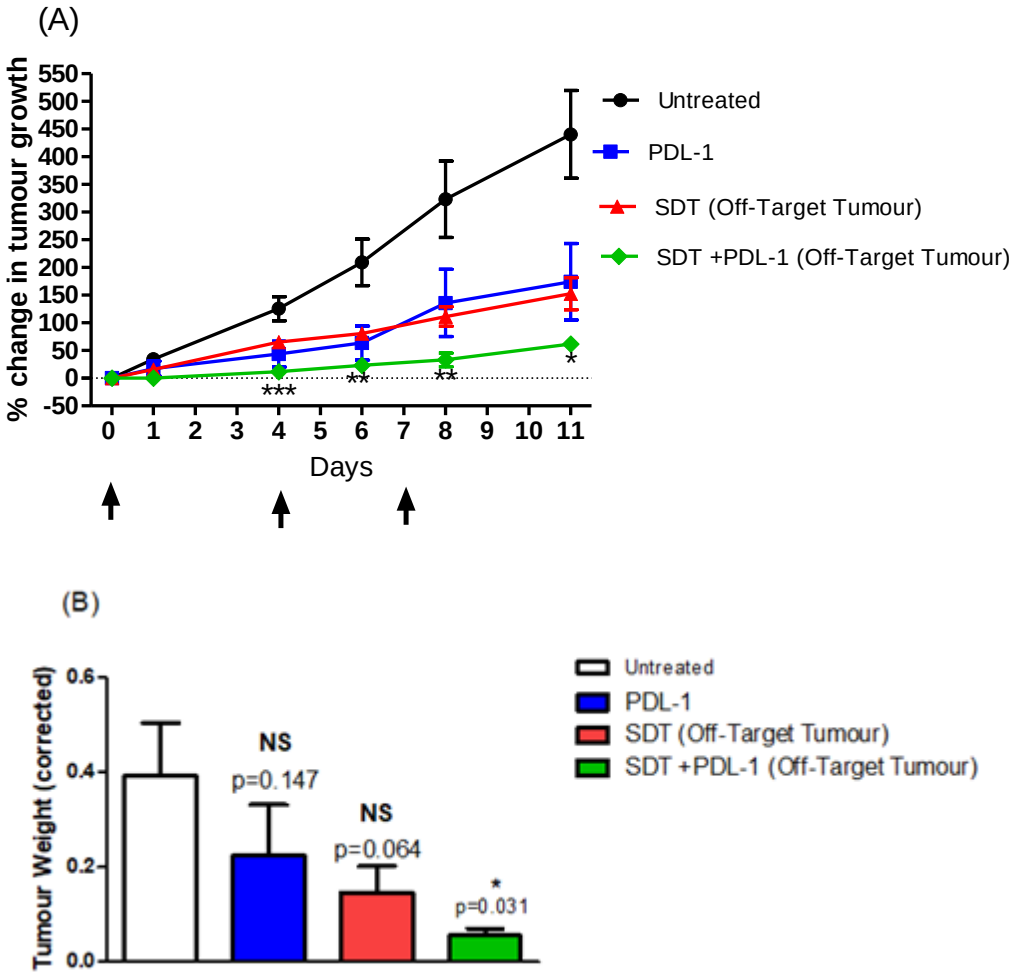

Figure 5 (A) Plot of % tumour volume for the off-target tumour in mice bearing bilateral T110299 pancreatic tumours that received (i) no treatment (ii) an IP injection of anti-PD-L1 antibody (iii) MB-RB conjugate + US at the primary tumour (SDT) and (iv) an IP injection of PD-L1 inhibitor 2 hours before treatment of the primary tumour with O_2MB-RB + US (PD-L1 + SDT). Animals treated on Days 0, 4 & 7. *p ≤ 0.05, **p ≤ 0.01, ***p ≤ 0.001 for PD-L1 + SDT v SDT. (B)Tumour mass at experimental endpoint (Day 11) in untreated, anti-PD-L1 and off target tumours of SDT and SDT + PD-L1 treated animals, n=4. *p ≤ 0.05 for T-test statistical analysis for each treatment group compared to untreated . Error bars represent ± SEM where n ≥4.

Figure 6 Representative images of animals from each group taken on Day 7 following initial treatment. The animals chosen had the same tumour volume at the start of the experiment.

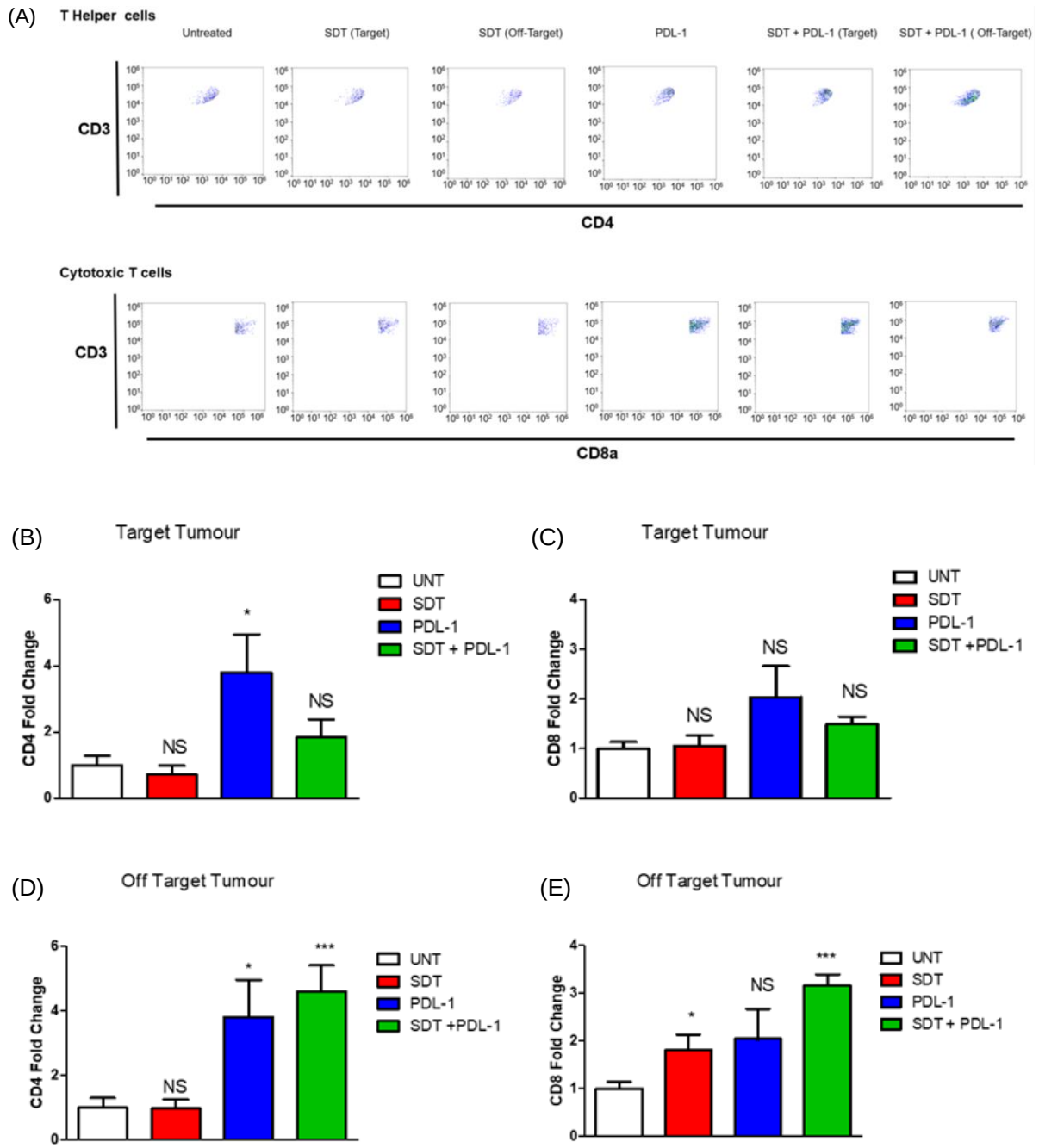

Figure 7 Flow cytometry dot plots (A) and Fold Change in CD4+ and CD8+ expression on day 11 (B, C) target tumours and (D, E) off-target tumours for untreated, anti-PDL-1, SDT and SDT + anti-PDL-1 treated animals, n=4. All groups were compared against untreated, *p ≤ 0.05, **p ≤ 0.01***p ≤ 0.001 for T-test statistical analysis. Error bars represent ± SEM where n ≥4.

Table 1 Flow cytometry data used to prepare Figure 6.

Treatment	Average CD4+ (% gated)	Average CD8+ (% gated)
Untreated Tumours	0.31	0.87
SDT Target Tumours	0.23	0.92
SDT Off Target Tumours	0.30	1.57
PD-L1 Tumours	1.19	1.78
SDT + PDL-1 Target Tumours	0.58	1.30
SDT + PDL-1 Off Target Tumours	1.44	2.75

References

[1] Paz-Ares, L., Luft, A., Vicente, D., Tafreshi, A., Gümüş, M., Mazières, J., Hermes, B., Çay Şenler, F., Csőszi, T., Fülöp, A. and Rodríguez-Cid, J., 2018. Pembrolizumab plus chemotherapy for squamous non–small-cell lung cancer. *New England Journal of Medicine*, *379*(21), pp.2040-2051.

[2] Schmid, P., Adams, S., Rugo, H.S., Schneeweiss, A., Barrios, C.H., Iwata, H., Diéras, V., Hegg, R., Im, S.A., Shaw Wright, G. and Henschel, V., 2018. Atezolizumab and nab-paclitaxel in advanced triple-negative breast cancer. *New England Journal of Medicine*, *379*(22), pp.2108-2121.

[3] Zhang, J.C., Chen, W.D., Alvarez, J.B., Jia, K., Shi, L., Wang, Q., Zou, N., He, K. and Zhu, H., 2018. Cancer immune checkpoint blockade therapy and its associated autoimmune cardiotoxicity. *Acta Pharmacologica Sinica*, *39*(11), pp.1693-1698.

[4] Tsai, H.F. and Hsu, P.N., 2017. Cancer immunotherapy by targeting immune checkpoints: mechanism of T cell dysfunction in cancer immunity and new therapeutic targets. *Journal of biomedical science*, *24*(1), p.35.

[5] Borghaei, H., Paz-Ares, L., Horn, L., Spigel, D.R., Steins, M., Ready, N.E., Chow, L.Q., Vokes, E.E., Felip, E., Holgado, E. and Barlesi, F., 2015. Nivolumab versus docetaxel in advanced nonsquamous non–small-cell lung cancer. *New England Journal of Medicine*, *373*(17), pp.1627-1639.

[6] Zappasodi, R., Merghoub, T. and Wolchok, J.D., 2018. Emerging concepts for immune checkpoint blockade-based combination therapies. *Cancer cell*, *33*(4), pp.581-598.

[7] Prasad, V. and Kaestner, V., 2017, April. Nivolumab and pembrolizumab: Monoclonal antibodies against programmed cell death-1 (PD-1) that are interchangeable. In *Seminars in oncology* (Vol. 44, No. 2, pp. 132-135). WB Saunders.

[8] Rizvi, N.A., Hellmann, M.D., Snyder, A., Kvistborg, P., Makarov, V., Havel, J.J., Lee, W., Yuan, J., Wong, P., Ho, T.S. and Miller, M.L., 2015. Mutational landscape determines sensitivity to PD-1 blockade in non–small cell lung cancer. *Science*, *348*(6230), pp.124-128.

[9] Kalita, N., Lord, J., Colquitt, J., Loveman, E., Scott, D.A. and Frampton, G., 2019. Cemiplimab for treating metastatic or locally advanced cutaneous squamous cell carcinoma: a Single Technology Appraisal.

[10] Akinleye, A. and Rasool, Z., 2019. Immune checkpoint inhibitors of PD-L1 as cancer therapeutics. *Journal of hematology & oncology*, *12*(1), p.92.

[11] Ventola, C.L., 2017. Cancer immunotherapy, part 3: challenges and future trends. *Pharmacy and Therapeutics*, *42*(8), p.514.

[12] Golden, E.B., Chhabra, A., Chachoua, A., Adams, S., Donach, M., Fenton-Kerimian, M., Friedman, K., Ponzo, F., Babb, J.S., Goldberg, J. and Demaria, S., 2015. Local radiotherapy and granulocyte-macrophage colony-stimulating factor to generate abscopal responses in patients with metastatic solid tumours: a proof-of-principle trial. *The lancet oncology*, *16*(7), pp.795-803.

[13] Marconi, R., Strolin, S., Bossi, G. and Strigari, L., 2017. A meta-analysis of the abscopal effect in preclinical models: Is the biologically effective dose a relevant physical trigger?. *PLoS One*, *12*(2).

[14] Choi, C., Yoo, G.S., Cho, W.K. and Park, H.C., 2019. Optimizing radiotherapy with immune checkpoint blockade in hepatocellular carcinoma. *World journal of gastroenterology*, *25*(20), p.2416.

[15] Reginato, E., Wolf, P. and Hamblin, M.R., 2014. Immune response after photodynamic therapy increases anti-cancer and anti-bacterial effects. *World journal of immunology*, *4*(1), p.1.

[16] Xu, J., Saklatvala, R., Mittal, S., Deshmukh, S. and Procopio, A., 2020. Recent Progress of potentiating immune checkpoint blockade with external stimuli—An industry perspective. *Advanced Science*, *7*(8), p.1903394.

[17] Li, X., Jeon, Y.H., Kwon, N., Park, J.G., Guo, T., Kim, H.R., Huang, J.D., Lee, D.S. and Yoon, J., 2021. In Vivo-assembled phthalocyanine/albumin supramolecular complexes combined with a hypoxia-activated prodrug for enhanced photodynamic immunotherapy of cancer. *Biomaterials*, *266*, p.120430.

[18] Wainwright, M., 2010. Therapeutic applications of near-infrared dyes. *Coloration Technology*, *126*(3), pp.115-126.

[19] Li, X., Lovell, J.F., Yoon, J. and Chen, X., 2020. Clinical development and potential of photothermal and photodynamic therapies for cancer. *Nature Reviews Clinical Oncology*, *17*(11), pp.657-674.

[20] Li, X., Lee, S. and Yoon, J., 2018. Supramolecular photosensitizers rejuvenate photodynamic therapy. *Chemical Society Reviews*, *47*(4), pp.1174-1188.

[21] Huang, H., Huang, D., Li, M., Yao, Q., Tian, R., Long, S., Fan, J. and Peng, X., 2020. NIR aza-pentamethine dyes as photosensitizers for photodynamic therapy. *Dyes and Pigments*, p.108284.

[22] Rapozzi, V., Beverina, L., Salice, P., Pagani, G.A., Camerin, M. and Xodo, L.E., 2010. Photooxidation and phototoxicity of π-extended squaraines. *Journal of medicinal chemistry*, *53*(5), pp.2188-2196.

[23] Lim, S.H., Thivierge, C., Nowak-Sliwinska, P., Han, J., Van Den Bergh, H., Wagnieres, G., Burgess, K. and Lee, H.B., 2010. In vitro and in vivo photocytotoxicity of boron dipyrromethene derivatives for photodynamic therapy. *Journal of medicinal chemistry*, *53*(7), pp.2865-2874.

[24] Avena, R.F., Qiao, L., Fujii, Y., Otomo, K., Ishii, H., Suzuki, T., Tsujino, H., Uno, T., Tsutsumi, Y., Kawashima, Y. and Takagi, T., 2020. Absorption, Fluorescence, and Two-Photon Excitation Ability of 5-Phenylisolidolo [2, 1-a] quinolines. *ACS omega*, *5*(5), pp.2473-2479.

[25] Wan, G.Y., Liu, Y., Chen, B.W., Liu, Y.Y., Wang, Y.S. and Zhang, N., 2016. Recent advances of sonodynamic therapy in cancer treatment. *Cancer biology & medicine*, *13*(3), p.325.

[26] Costley, D., Mc Ewan, C., Fowley, C., McHale, A.P., Atchison, J., Nomikou, N. and Callan, J.F., 2015. Treating cancer with sonodynamic therapy: a review. *International Journal of Hyperthermia*, *31*(2), pp.107-117.

[27] Nomikou, N., Fowley, C., Byrne, N.M., McCaughan, B., McHale, A.P. and Callan, J.F., 2012. Microbubble–sonosensitiser conjugates as therapeutics in sonodynamic therapy. *Chemical communications*, *48*(67), pp.8332-8334.

[28] Zhang, Q., Bao, C., Cai, X., Jin, L., Sun, L., Lang, Y. and Li, L., 2018. Sonodynamic therapy-assisted immunotherapy: A novel modality for cancer treatment. *Cancer science*, *109*(5), pp.1330-1345.

[29] McEwan, C., Kamila, S., Owen, J., Nesbitt, H., Callan, B., Borden, M., Nomikou, N., Hamoudi, R.A., Taylor, M.A., Stride, E. and McHale, A.P., 2016. Combined sonodynamic and antimetabolite therapy for the improved treatment of pancreatic cancer using oxygen loaded microbubbles as a delivery vehicle. *Biomaterials*, *80*, pp.20-32.

[30] Nesbitt, H., Sheng, Y., Kamila, S., Logan, K., Thomas, K., Callan, B., Taylor, M.A., Love, M., O'Rourke, D., Kelly, P. and Beguin, E., 2018. Gemcitabine loaded microbubbles for targeted chemo-sonodynamic therapy of pancreatic cancer. *Journal of controlled release*, *279*, pp.8-16.

[31] Logan, K., Foglietta, F., Nesbitt, H., Sheng, Y., McKaig, T., Kamila, S., Gao, J., Nomikou, N., Callan, B., McHale, A.P. and Callan, J.F., 2019. Targeted chemo-sonodynamic therapy treatment of breast tumours using ultrasound responsive microbubbles loaded with paclitaxel, doxorubicin and Rose Bengal. *European journal of pharmaceutics and biopharmaceutics*, *139*, pp.224-231.

[32] Feng, M., Xiong, G., Cao, Z., Yang, G., Zheng, S., Song, X., You, L., Zheng, L., Zhang, T. and Zhao, Y., 2017. PD-1/PD-L1 and immunotherapy for pancreatic cancer. *Cancer letters*, *407*, pp.57-65.

[33] Brahmer, J.R., Tykodi, S.S., Chow, L.Q., Hwu, W.J., Topalian, S.L., Hwu, P., Drake, C.G., Camacho, L.H., Kauh, J., Odunsi, K. and Pitot, H.C., 2012. Safety and activity of anti–PD-L1 antibody in patients with advanced cancer. *New England Journal of Medicine*, *366*(26), pp.2455-2465.

[34] Nomi, T., Sho, M., Akahori, T., Hamada, K., Kubo, A., Kanehiro, H., Nakamura, S., Enomoto, K., Yagita, H., Azuma, M. and Nakajima, Y., 2007. Clinical significance and therapeutic potential of the programmed death-1 ligand/programmed death-1 pathway in human pancreatic cancer. *Clinical cancer research*, *13*(7), pp.2151-2157.

[35] Hosein, A.N., Brekken, R.A. and Maitra, A., 2020. Pancreatic cancer stroma: an update on therapeutic targeting strategies. *Nature Reviews Gastroenterology & Hepatology*, pp.1-19.

[36] Knudsen, E.S., Vail, P., Balaji, U., Ngo, H., Botros, I.W., Makarov, V., Riaz, N., Balachandran, V., Leach, S., Thompson, D.M. and Chan, T.A., 2017. Stratification of pancreatic ductal adenocarcinoma: combinatorial genetic, stromal, and immunologic markers. *Clinical Cancer Research*, *23*(15), pp.4429-4440.

[37] McEwan, C., Owen, J., Stride, E., Fowley, C., Nesbitt, H., Cochrane, D., Coussios, C.C., Borden, M., Nomikou, N., McHale, A.P. and Callan, J.F., 2015. Oxygen carrying microbubbles for enhanced sonodynamic therapy of hypoxic tumours. *Journal of Controlled Release*, *203*, pp.51-56.

[38] Kooiman, K., Vos, H.J., Versluis, M. and de Jong, N., 2014. Acoustic behavior of microbubbles and implications for drug delivery. *Advanced drug delivery reviews*, *72*, pp.28-48.

[39] Xing, L., Shi, Q., Zheng, K., Shen, M., Ma, J., Li, F., Liu, Y., Lin, L., Tu, W., Duan, Y. and Du, L., 2016. Ultrasound-mediated microbubble destruction (UMMD) facilitates the delivery of CA19-9 targeted and paclitaxel loaded mPEG-PLGA-PLL nanoparticles in pancreatic cancer. *Theranostics*, *6*(10), p.1573.

[40] Sennoga, C.A., Mahue, V., Loughran, J., Casey, J., Seddon, J.M., Tang, M. and Eckersley, R.J., 2010. On sizing and counting of microbubbles using optical microscopy. *Ultrasound in medicine & biology*, *36*(12), pp.2093-2096.

[41] Adunka, T., 2014. Characterization of murine pancreatic carcinoma models regarding immunosuppressive mechanisms and therapy with bifunctional siRNA targeting galectin-1 (Doctoral dissertation, lmu).

[42] Xu, N., Du, J., Yao, Q., Ge, H., Li, H., Xu, F., Gao, F., Xian, L., Fan, J. and Peng, X., 2020. Precise photodynamic therapy: Penetrating the nuclear envelope with photosensitive carbon dots. *Carbon*, *159*, pp.74-82.

[43] Zheng, Y., Yin, G., Le, V., Zhang, A., Chen, S., Liang, X. and Liu, J., 2016. Photodynamic-therapy activates immune response by disrupting immunity homeostasis of tumor cells, which generates vaccine for cancer therapy. *International journal of biological sciences*, *12*(1), p.120.

[44] Lanitis, E., Dangaj, D., Irving, M. and Coukos, G., 2017. Mechanisms regulating T-cell infiltration and activity in solid tumors. *Annals of Oncology*, *28*(suppl_12), pp.xii18-xii32.

[45] Iwai, Y., Ishida, M., Tanaka, Y., Okazaki, T., Honjo, T. and Minato, N., 2002. Involvement of PD-L1 on tumor cells in the escape from host immune system and tumor immunotherapy by PD-L1 blockade. *Proceedings of the National Academy of Sciences*, *99*(19), pp.12293-12297.

[46] Chiu, Y.M., Tsai, C.L., Kao, J.T., Hsieh, C.T., Shieh, D.C., Lee, Y.J., Tsay, G.J., Cheng, K.S. and Wu, Y.Y., 2018. PD-1 and PD-L1 up-regulation promotes T-cell apoptosis in gastric adenocarcinoma. *Anticancer research*, *38*(4), pp.2069-2078.

[4] Miksch, R.C., Schoenberg, M.B., Weniger, M., Bösch, F., Ormanns, S., Mayer, B., Werner, J., Bazhin, A.V. and D'Haese, J.G., 2019. Prognostic impact of tumor-infiltrating lymphocytes and neutrophils on survival of patients with upfront resection of pancreatic cancer. *Cancers*, *11*(1), p.39.

[48] Tong, H., Fan, Z., Liu, B. and Lu, T., 2018. The benefits of modified FOLFIRINOX for advanced pancreatic cancer and its induced adverse events: a systematic review and meta-analysis. *Scientific reports*, *8*(1), pp.1-8.

[49] Gresham, G.K., Wells, G.A., Gill, S., Cameron, C. and Jonker, D.J., 2014. Chemotherapy regimens for advanced pancreatic cancer: a systematic review and network meta-analysis. *BMC cancer*, *14*(1), p.471.

[50] Tachibana, K., Feril Jr, L.B. and Ikeda-Dantsuji, Y., 2008. Sonodynamic therapy. *Ultrasonics*, *48*(4), pp.253-259.